FUNCTION™ american physiological society

*FUNCTION*, 2022, 3(3): zqac015

https://doi.org/10.1093/function/zqac015
Advance Access Publication Date: 24 March 2022
Original Research

RESEARCH ARTICLE

# Mechanotherapy Reprograms Aged Muscle Stromal Cells to Remodel the Extracellular Matrix during Recovery from Disuse

Zachary R. Hettinger[1,2,†], Yuan Wen[2,3], Bailey D. Peck[1,2], Kyoko Hamagata[2], Amy L. Confides[1,2], Douglas W. Van Pelt[1,2], Douglas A. Harrison[4], Benjamin F. Miller[5], Timothy A. Butterfield[2,6], Esther E. Dupont-Versteegden[1,2,*]

[1]Department of Physical Therapy, College of Health Sciences, University of Kentucky, Lexington, KY 40536, USA, [2]Center for Muscle Biology, University of Kentucky, Lexington, KY 40536, USA, [3]Department of Physiology, College of Medicine, University of Kentucky, Lexington, KY 40536, USA, [4]Department of Biology, College of Arts and Sciences, University of Kentucky, Lexington, KY 40536, USA, [5]Aging and Metabolism Research Program, Oklahoma Medical Research Foundation, Oklahoma City, OK 73104, USA and [6]Department of Athletic Training and Clinical Nutrition, College of Health Sciences, University of Kentucky; Lexington, KY 40536, USA

*Address correspondence to EED-V (e-mail: Esther.dupont@uky.edu)
†Current Institution: McGowen Institute for Regenerative Medicine, University of Pittsburgh, Pittsburgh, PA, 15219

## Abstract

Aging is accompanied by reduced remodeling of skeletal muscle extracellular matrix (ECM), which is exacerbated during recovery following periods of disuse atrophy. Mechanotherapy has been shown to promote ECM remodeling through immunomodulation in adult muscle recovery, but not during the aged recovery from disuse. In order to determine if mechanotherapy promotes ECM remodeling in aged muscle, we performed single cell RNA sequencing (scRNA-seq) of all mononucleated cells in adult and aged rat gastrocnemius muscle recovering from disuse, with (REM) and without mechanotherapy (RE). We show that fibroadipogenic progenitor cells (FAPs) in aged RE muscle are highly enriched in chemotaxis genes (*Csf1*), but absent in ECM remodeling genes compared to adult RE muscle (*Col1a1*). Receptor-ligand (RL) network analysis of all mononucleated cell populations in aged RE muscle identified chemotaxis-enriched gene expression in numerous stromal cell populations (FAPs, endothelial cells, pericytes), despite reduced enrichment of genes related to phagocytic activity in myeloid cell populations (macrophages, monocytes, antigen presenting cells). Following mechanotherapy, aged REM mononuclear cell gene expression resembled adult RE muscle as evidenced by RL network analyses and KEGG pathway activity scoring. To validate our transcriptional findings, ECM turnover was measured in an independent cohort of animals using *in vivo* isotope tracing of intramuscular collagen and histological scoring of the ECM, which confirmed mechanotherapy-mediated ECM remodeling in aged RE muscle. Our results highlight age-related cellular

**Submitted:** 22 January 2022; **Revised:** 2 March 2022; **Accepted:** 8 March 2022

mechanisms underpinning the impairment to complete recovery from disuse, and also promote mechanotherapy as an intervention to enhance ECM turnover in aged muscle recovering from disuse.

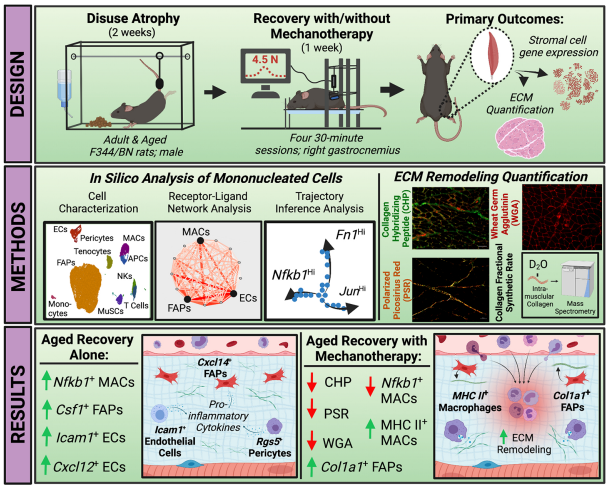


**Key words:** Aging; skeletal muscle; mechanotherapy; single cell RNA sequencing; disuse atrophy; reloading

## Introduction

The recovery of skeletal muscle following disuse atrophy is impaired in older adults, which results in increased vulnerability to reduced physical function and poor quality of life.[1–3] A mechanistic understanding of hampered regrowth in aged skeletal muscle, along with clinically available interventions for a vulnerable patient population, are therefore needed. In the present study, we demonstrate that mechanotherapy in the form of cycling compressive loading, a massage mimetic, reprograms the transcriptomes of numerous muscle stromal cell populations in order to promote remodeling of the extracellular matrix (ECM), thereby creating a microenvironment that is more favorable to regrowth in aged muscle recovering from disuse atrophy.

Recovery from atrophy following a period of disuse in adult muscle is characterized by a transient infiltration of immune cells,[4] removal of cellular and ECM-related debris[5] and deposition of newly synthesized ECM components.[6] These processes are needed for regrowth, but are complicated in aged muscle because of the impairment to ECM regulation, evidenced by a fibrotic morphology[7] and elevated passive stiffness.[8] ECM in aged muscle is characterized by protein compositional shifts that ultimately influence the mechanotransduction of resident cell populations, thereby affecting their function.[8–11] Importantly, promotion of ECM remodeling in aged muscle results in an enhanced ability for muscle to respond to loading and increase in size.[12] Regulation of skeletal muscle ECM is dependent on resident and infiltrating cell populations, which include both fibroadipogenic progenitor cells (FAPs)[13,14] and macrophages,[15] among others. Disruption of macrophage and FAP crosstalk results in impaired muscle function and aberrant ECM organization.[13,16] Indeed, there are increasing reports of the deleterious role stromal cells may play in aging skeletal muscle, such as contributing to muscle insulin resistance[17] and dissolution of the satellite cell niche.[14] These findings suggest that aged muscle stromal cells may contribute to the impaired recovery from disuse atrophy in aged individuals by changing the ECM. However, neither intracellular crosstalk between stromal and infiltrating cell populations nor therapies to promote ECM turnover in aged muscle recovering from disuse have been reported.

Massage has been used as a mechanotherapy to alleviate muscle dysfunction and promote well-being for thousands of years,[18–20] but mechanisms underlying the beneficial effects have only more recently been reported.[21–23] Our laboratory has identified cyclic compressive loading, a massage mimetic, to be a mechanotherapy for skeletal muscle,[24] by enhancing muscle anabolic signaling,[25] stimulating satellite cell proliferation,[26] and by promoting immunomodulation.[22,23] Indeed, mechanotherapy attenuates skeletal muscle immune cell accumulation following damage-induced eccentric exercise, leading to accelerated recovery and increased muscle function in rabbits.[23] Similar findings have been shown in humans using massage therapy following a damaging bout of exercise, albeit through unknown cellular mechanisms.[21] The clinical potential of mechanotherapy to augment recovery in aged individuals is promising due to the vulnerability of this patient population and the decreased ability to perform more common muscle strengthening exercises to accelerate recovery.

In this study, we hypothesized that mechanotherapy stimulated stromal cell populations to remodel the ECM in aged muscles recovering from disuse atrophy. We leveraged single cell RNA-sequencing of muscle mononucleated cells, histochemical evaluation of the ECM, and *in vivo* isotope tracing of intramuscular collagen to demonstrate that mechanotherapy is immunomodulatory to aged muscle recovering from disuse atrophy, by mechanically reprogramming both stromal and infiltrating cell populations to transcriptomes favorable to ECM remodeling. Functionally, we demonstrate that mechanotherapy causes turnover of numerous ECM components, thereby creating a microenvironment more permissive to recovery. Altogether, our results highlight intercellular mechanisms contributing to the age-related impairment to ECM remodeling during the recovery from disuse, and also identifies mechanotherapy as a novel intervention to promote ECM remodeling in aged muscles recovering from disuse atrophy.

## Experimental Procedures

### Study Design

#### *Animals*

Ethical approval for all experimental procedures was provided by the Institutional Animal Care and Use Committee at the University of Kentucky. Experiments were performed in accordance with guidelines outlined by the National Research Council's *Guide for the Care and Use of Laboratory Animals: Eighth Edition* and ARRIVE guidelines. Male Fisher 344 X Brown Norway (F344/BN) rats at 10- (adult) and 30-months of age (aged) were randomly assigned to the following groups: weight bearing (WB), recovery after atrophy (RE) and recovery after atrophy with mechanotherapy (REM). Six rats were used for scRNA-seq experiments with each group containing one rat and the *N* was considered as individual cells. For histological evaluation of the ECM, n = 6-8 muscles were used for each group.

#### *Hindlimb Suspension*

Following a week of acclimation, F344/BN rats were either allowed to ambulate freely around their cage (WB) or were subjected to hindlimb suspension (HS) for 14 days followed by 7 days of free ambulation with (REM) or without mechanotherapy (RE). HS was performed as previously described.[25,27–29] Briefly, a metal wire with ring attachment was secured to the base of the tail using cyanoacrylate glue and surgical gauze while the rats were anesthetized (2% isoflurane by inhalation). Rats were placed in single-housed custom-built cages with tall walls and a metal rod traversing the length of the cage, and were raised gradually for the first 24 hours to minimize stress, and monitored daily until termination of HS. Following 14 days of HS the rats were anesthetized (2% isoflurane by inhalation), the suspension apparatus was removed, and rats were allowed to ambulate freely for a total of 7 days to begin muscle mass recovery. These times points were chosen to be able to compare our results to our previous study in adult and aged rats.[25,30,31]

#### *Mechanotherapy*

Mechanotherapy in the form of cyclic compressive loading, a massage mimetic, was performed on gastrocnemius muscles recovering from disuse using procedures described previously.[22,25,27,28] Briefly, mechanotherapy consisted of four 30-minute bouts of cyclic compressive loading at 4.5 N load and 0.5Hz duty cycle to the right gastrocnemius muscle every other day during the recovery period starting at the time of reloading. During the mechanotherapy, rats were anesthetized (2% isoflurane by inhalation) and placed left lateral recumbent on a heated sling prior to securing the hindlimb to the stage by taping the talocrural joint. A spring-loaded cylinder with attached force transducer was then set to roll over the right hindlimb, which allows for real-time visual feedback of mechanotherapy load and frequency. Rats not receiving mechanotherapy were anesthetized (2% isoflurane by inhalation) and placed on a heated pad for a total of 30 minutes every other day (total of 4 bouts) to control for potential confounding effects of anesthesia. Afterwards, all rats were allowed to recover on a heated pad before returning to their cages. This protocol was chosen as it was shown previously to increase muscle fiber cross sectional area and myofibrillar protein synthesis in adult but not aged rats.[25,30]

#### *Deuterium Oxide Labeling*

Rats were provided with deuterium oxide ($D_2O$) to isotopically label intramuscular collagen as described previously.[25,27,32] Briefly, rats in the WB group received a bolus of $D_2O$ via IP injection (99%; equivalent to 5% of the body water pool), followed by provision of $D_2O$-enriched drinking water (8%) for the remainder of the experiment (Figure 1A). Rats in both the RE and REM group received a bolus of $D_2O$ via IP injection (99%; equivalent to 5% of the body water pool) two days prior to termination of HS and were provided with $D_2O$-enriched drinking water (8%) for the remainder of the experiment (Figure 1A).

#### *Tissue Collection*

Rats used for scRNA-seq were euthanized four hours after the last bout of mechanotherapy or sham treatment by intraperitoneal injection (IP) (Somnasol™, Euthansia III solution; 150 mg $g^{-1}$) and exsanguination. Gastrocnemius muscles were immediately harvested and subjected to cell isolation as described below. Rats used for (immuno)histochemistry and collagen synthesis analyses were euthanized 24 h after the last bout of mechanotherapy by IP injection (Somnasol™, Euthansia III solution; 150 mg $g^{-1}$) and exsanguination. Blood was collected by cardiac puncture before exsanguination and subjected to centrifugation (2000 g, 10 min, 4°C) for serum isolation, and stored at -80°C for future analyses. Gastrocnemius muscles were harvested and placed on cards, flash frozen in liquid nitrogen, and stored at −80°C for future analyses.

### Single Cell RNA Sequencing

#### *Cell Isolation, Flow-Cytometry, and scRNA-Sequencing*

Live mononuclear cells were isolated from the right gastrocnemius muscle as previously described.[33] Briefly, right gastrocnemius muscle was immersed in wash media (WM; Ham's F-10 (Gibco, Gaithersburg, Maryland) + 10% Horse serum (Thermo Fisher, Florence, KY) and 1X penicillin/streptomycin (Gibco)) immediately after dissection and minced using sterilized instruments. The minced muscle homogenate was incubated in muscle dissociation media (MDM; WM + 800 U/ml Collagenase II (Gibco)) at 37°C for 1 h with agitation. The homogenate was pelleted by centrifugation (500g, 5 min) and incubated in fresh MDM supplemented with dispase (11 U/ml; Sigma, St. Louis, MO) at 37°C for 30 min with agitation. The single cell suspension was pelleted by centrifugation (500 g, 5 min), passed through 70- and 40-$\mu$m Nylon cell strainers to remove non-cellular material, and placed in a fluorescence-activated cell sorting (FACS) tube containing propidium iodide (PI) and WM to identify dead cells. Isolation of live mononuclear cells was performed by gating out cellular debris using forward/side scatter and with/without PI using an iCyt FACS (Sony Biotechnology, Champaign, IL, USA). The mononuclear cell pellet was washed and resuspended in PBS with 0.04% BSA in accordance with 10X Genomics recommendations (10X Genomics, Pleasanton, CA, USA). Concentration of cells was determined using a hematocytometer and viability was determined using acridine orange/ethidium homodimer. Cells were loaded in the 10X Genomics Chromium Controller to target capture of approximately 10,000 cells per lane using the Single Cell 3' reagent kit per the manufacturer's instructions. Libraries were made using version 3.0 chemistry and sequenced on an Illumina HiSeq platform (Novogene, Sacramento, CA), yielding a minimum 200 million reads per sample.

#### *Data Processing and Visualization*

Sequencing, quality control and visualization of reads was performed using the Partek Genomics Suite (Partek, St. Louis, MO, USA) for scRNA-seq as recommended by manufacturer's instructions. Briefly, FASTQ files were imported into Partek Flow and

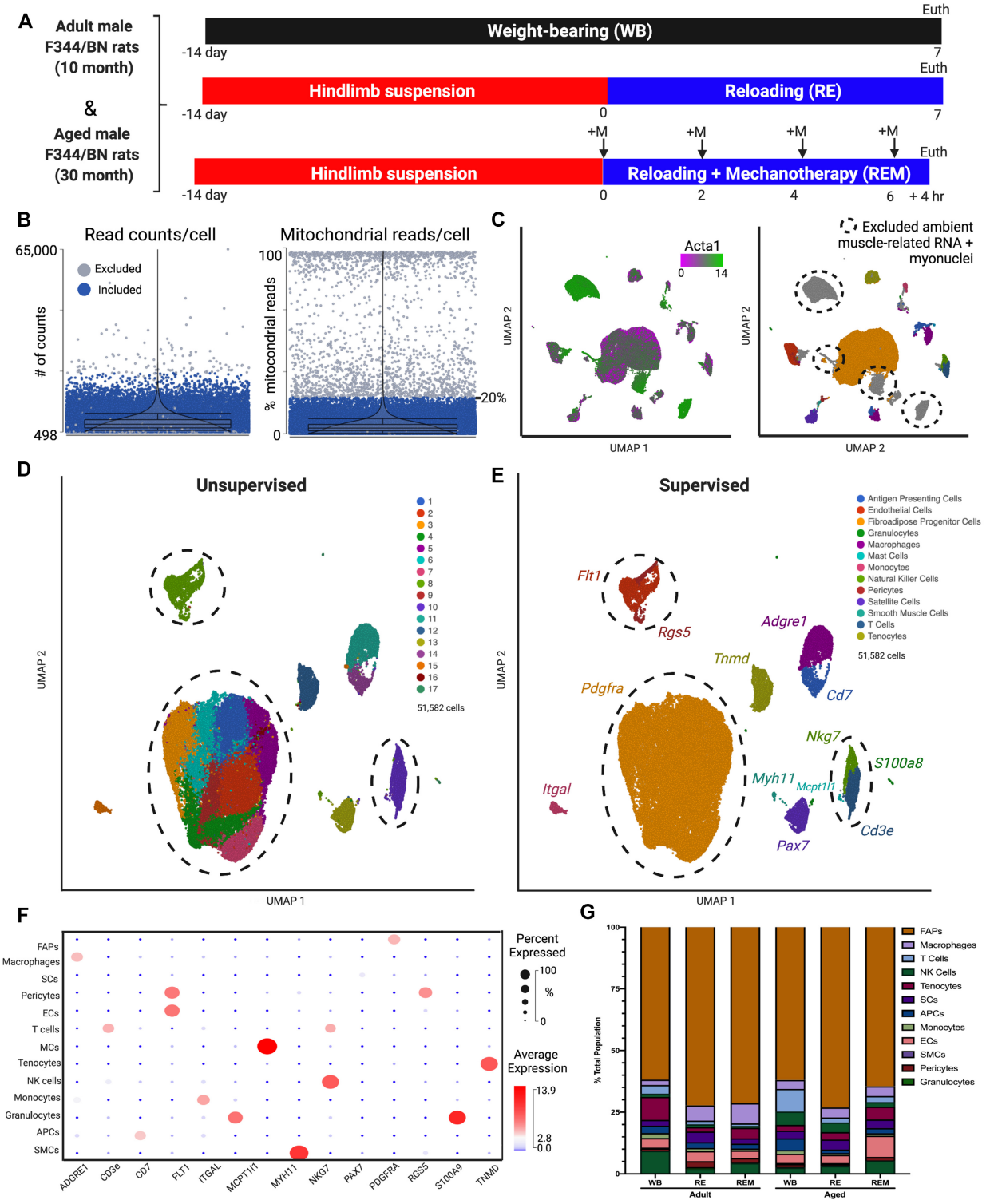


**Figure 1.** Transcriptional heterogeneity of muscle resident cell populations during the recovery from disuse atrophy. (A) experimental design of 10- (adult) and 30-month (aged) F344/BN rats randomized into weight-bearing (WB), reloading following hindlimb suspension (RE), and reloading supplemented with mechanotherapy (REM) groups. +M: mechanotherapy. Euth; euthanasia. N = 1 rat gastrocnemius/group. (B) Quality assessment (QA) of cells based on total read counts (doublets) and percentages of expressed mitochondrial reads per cell. Cells colored in blue included for analysis. Cells colored in gray did not pass QA filters (<20% mitochondrial gene expression). (C) Following QA, UMAP visualization of ambient actin alpha 1 (*Acta1*; green) infiltrated within mononuclear cell populations from muscle harvesting. Mononuclear cells included for analysis (colored) versus cells removed based on QA and ambient RNA infiltration (grey). (D) Unsupervised graph-based clustering and (E) supervised clustering of aggregate samples (51,582 cells total from all groups combined) visualized UMAP. Discrepancies in clustering highlighted by dashed circles. (F) Bubble plot of genes selected for supervised-based classification corresponding to each identified cell population using selected markers. Average gene expression is denoted by heat map and the non-zero percent of cells expressing the gene is denoted by bubble size. (G) The percentages of each cell population per sample identified by supervised-based cell classification.

reads were mapped to the rn6 rat assembly. Low quality cells were removed based on number of read counts, high percentage of mitochondrial reads (>10%), and low number of detected genes per cell (minimum of 500 genes). For data normalization, reads were normalized by counts per million and log transformed. Noise reduction was performed for genes considered to be background by excluding genes that had a value of 0 in at least 99.9% of cells. Dimensionality reduction was performed using PCA, and visualization performed by UMAP. Bubble plots to visualize the specificity of genes to various cell populations were generated by measuring the average expression value of the gene of interest (indicated by heat map) and also by the percentage of cells within a given population expressing the gene of interest (indicated by bubble size). The mononuclear cell isolation method results in the release of muscle fiber-related RNA that is considered ambient in this experiment, and therefore cells containing high expression of muscle fiber-specific genes were excluded from analyses. Following QC, a total of 51,582 cells were obtained for downstream analyses.

## *In silico* Analyses

### *Cluster Annotation*

Cluster annotation was performed using both supervised and unsupervised methods. Graph-based clustering was performed following dimensionality reduction, and unique biomarkers for each cluster were calculated using a rank-sum test that compares cells in a specific cluster to those in all other clusters. Supervised annotation of clusters was performed using published gene expression data and compared to unsupervised labeling. Dimensionality reduction, graph-based clustering, and UMAP visualization on cell types of interest was performed to identify subclusters.

### *Receptor-Ligand Network Analysis*

Receptor-ligand interaction networks were generated using the unique gene lists per cell population and sample against a curated receptor-ligand dataset.[34,35] Prior to analysis, unique gene lists were filtered based on a log-fold change of 3.0 or higher to minimize non-significant cell–cell interactions. Significant interactions were computed using the number of significant interactions between cell populations along with the average expression of the particular ligand/receptor.

### *Pathway Activity Scoring*

AuCell[36] was used to calculate pathway activity scores (Z scores) from downloaded KEGG datasets (https://www.genome.jp/kegg/brite.html). Average activity score is indicated by heat map (higher activity scores are highlighted in red, lower scores highlighted in blue). Single cell macrophage expression of selected pathways is shown by individual bars.

### *Trajectory Analysis*

Monocle 3.0 was used for trajectory inference and pseudotime analyses[37,38] (Partek Flow). *Adgre1*+ cells (macrophages) from all samples were subjected to trajectory analysis following data normalization and preprocessing. Gene count matrices were log2 transformed and projected into the top 50 principal components, followed by dimensionality reduction and visualization using UMAP. States, branch points, and pseudotime values were calculated and added to the trajectory plot.

## Collagen Synthesis

### *Fractional Synthesis Rate*

Collagen fractional synthesis rate (FSR) was determined as previously described.[25,27,39] Briefly, muscles were ground to a powder in liquid nitrogen, placed in homogenization buffer (0.15 M NaCL, 0.1% Triton X-100, and 0.02 M Tris-HCl pH 7.4), and centrifuged prior to differential salt extraction. The supernatant was removed and KCl (0.7 M) was added to the pellet followed by a second centrifugation. The remaining collagen pellet was washed with 0.5 M acetic acid followed by acetic acid-pepsin (0.1% w/v). Isolated and purified collagens were added to 250 $\mu$l 1 M NaOH and incubated for 15 min at 50°C with gentle agitation. Proteins were hydrolyzed by adding 6 N HCl overnight at 120°C. The pentafluorobenzyl-N,N-di (pentafluorobenzyl) derivative of alanine was measured on an Agilent 7890A GC (Agilent, Santa Clara, USA) coupled to an Agilent 5975C MS (Agilent). Body water enrichment was calculated by placing 125 $\mu$l of serum into the inner well of o-ring screw cap and then placed onto a heat block overnight. The following day, 2 $\mu$l of 10 M NaOH and 20 $\mu$l acetone was added to samples and $D_2O$ standards, vortexed, and left to incubate overnight at RT. Extractions were performed using hexane and the organic layer was isolated and placed into gas spectrometry vials for analysis using electron impact mode. The newly synthesized fraction of collagens was calculated by dividing the enrichment of alanine-bound collagens by the true precursor enrichment, while using plasma $D_2O$ enrichment with mass isotopomer distribution analysis adjustment.[25,32]

## Histochemical Analyses

Collagen hybridizing peptide (CHP) staining was performed per manufacturer's instructions and modified for rat. Briefly, 8 $\mu$m gastrocnemius muscle sections were fixed in acetone (-20°C) for 10 min, and then washed in PBS. Stock Collagen 3Helix-Biotin Peptide (50 $\mu$M; B-CHP #BIO-300; 3Helix, Salt Lake City, UT) was diluted in PBS (20$\mu$M), placed on a heating block (80°C) for 5 min and quickly cooled on wet ice for 1 min. CHP was added to sections and incubated overnight at 4°C. Slides were washed in PBS and incubated in AlexaFlour 488 (1:500) for 30 min at RT. To visualize CHP relative to the total extracellular area, slides were co-stained with wheat germ agglutinin (Invitrogen, #W21405; 1:50) for 2 h at RT. Slides were washed, mounted using Vectashield Fluorescent mounting medium (Vector Labs; #H-1000), and coverslipped. Five regionally representative images containing a minimum of 500 muscle fibers per muscle were taken using a Zeiss upright microscope (AxioImager M1, Oberkochen, Germany) and averaged for each rat. Thresholding of CHP and WGA and muscle fiber counts were performed by a blinded assessor using Zen 2.0 imaging analysis software. Picrosirius red (PSR) staining was performed according to previous studies,[40] with modifications for rat muscle. Briefly, muscle sections were fixed with 4% paraformaldehyde for 30 min at RT, followed by placing the slides vertical to air dry for 30 min at RT. Sections were incubated in PSR solution (0.1% PSR in saturated picric acid; Electron Microscopy Sciences, Hatfield, PA) for 1 h rocking at RT. Sections were washed, dehydrated with ethanol, and mounted with xylene-based mounting media. An average of 5-6 representative images (minimum of 500 fibers per muscle) were taken on an upright microscope (AxioImager M1, Oberkochen, Germany Zeiss) and subjected to circularly polarized light as previously described.[8,41] Images were analyzed using publicly available Image J plugin Colored Pixel Counter. The sum of red, green,

and yellow pixels was measured and reported relative to total pixels in the image.

### Statistical Analyses

CHP, WGA, PSR-Polarization, and collagen FSR data were assessed for normality and equal variance using GraphPad Prism; all data presented were normally distributed and passed tests for equal variance. A one-way ANOVA with condition as a variable was used to detect statistical significance in each age group, followed by a Tukey's post hoc test for multiple comparisons; the effect of age on muscle ECM has been reported previously.[8] Statistical significance was assumed at $P < 0.05$. The gene specific analysis feature of Partek Flow, followed by FDR step-up ($q<0.05$) to control for multiple comparisons, was used to generate differentially expressed genes between selected comparisons.

## Results

### The Transcriptional Landscape of Skeletal Muscle Recovering from Disuse Atrophy

We performed single cell RNA sequencing (scRNA-seq) on gastrocnemius muscles from F344/BN rats at 10 (adult) and 30 (aged) months of age to characterize the transcriptional landscape of mononuclear cells during recovery from atrophy with and without mechanotherapy, as previously described[27,30,31] (Figure 1A). Following two weeks of hindlimb suspension (unloading) to induce disuse atrophy of the gastrocnemius muscle, rats were allowed to ambulate freely (reloading: RE) for a period of 7 days, with or without mechanotherapy (REM) (Figure 1A). Seven days of recovery was chosen to be able to compare findings from the current study to our previously published studies.[30,31] We also included ambulatory WB rats at each age to determine whether aging alone was associated with differences in gene expression of cells responsible for ECM regulation. Following muscle harvesting, cellular isolation, removal of debris and dead cells, live cells were isolated via fluorescent-activated cell sorting (FACS)[33] (Figure 1A). Following sequencing and alignment, cells were filtered for "quality", based on mitochondrial read percentages (>20%) and reads/cell as recommended by Partek Genomics (Figure 1B). Low quality cells share similar features of high mitochondrial read percentages, lower detected genes per cell, and higher numbers of read counts per cells (indicative of doublets), and therefore can be removed before downstream analyses (Figure 1B). Moreover, as the isolation of muscle mononuclear cells results in release of myofiber-related RNA that becomes "sticky" during isolation, removal of mononucleated cells enriched with ambient muscle RNA (Actin alpha 1 (*Acta1*); green) is essential prior to downstream analyses (Figure 1C). Lastly, myonuclei were also excluded due to loss of cytoplasmic transcripts during muscle mincing (Figure 1C; *Acta1*; green on left panel, grey on right panel). Following quality assessment, a total of 51,582 cells across 6 conditions were obtained for downstream analyses.

To visualize the data, we performed dimensionality reduction using principal component analysis (PCA), followed by clustering of the aggregated dataset comprised of all samples, and data visualization using uniform manifold approximation projection (UMAP). Graph-based clustering (unsupervised) identified a total of 17 clusters across all groups (Figure 1D), which we compared to manual cluster identification (supervised) using frequently reported gene markers[35,42–44] (Figure 1E). To ensure that clustering was not the result of batch effect, individual PCAs, UMAP visualization and cluster annotation were performed on each sample individually prior to analyzing the aggregate dataset (data not shown). Using cell-specific gene markers, we identified a total of 13 cell populations including pericytes (*Rgs5*+), endothelial cells (ECs; *Flt1*+), tenocytes (*Tnmd*+), FAPs (*Pdgfra*+), monocytes (*Itgal*+), T cells (*Cd3e*+), natural killer cells (*Nkg7*+), mast cells (*Mcpt1l1*+), satellite cells (*Pax7*+), macrophages (*Adgre1*+), antigen presenting cells (*Cd7*+), granulocytes (*S100a8*+), and smooth muscle cells (*Myh11*+) (Figure 1E). We identified discrepancies between graph-based (unsupervised) and manual cell population annotation (supervised) in ECs, FAPs, and pericytes by comparing results from supervised and unsupervised annotation strategies (Figure 1B, 1C; indicated by dashed circles). Graph-based annotation of cells did not identify transcriptional differences between ECs and pericytes, combining them into a single cluster, demonstrating an inability of unsupervised clustering to detect transcriptional differences between the two cell populations (Figure 1B, 1C; indicated by dashed circles). Moreover, a total of 8 subclusters were identified within FAPs, demonstrating the precision and sensitivity of supervised clustering compared to unsupervised clustering in this study (Figure 1B, 1C; indicated by dashed circles). For reference, a bubble plot is provided for evidence that the gene markers selected for supervised annotation are highly specific for the identified cell populations (Figure 1F; bubble size indicates percent of cells expressing, heatmap indicates average expression). In the absence of myofibers, the predominant cell population isolated from the single cell suspension was FAPs, followed by ECs, macrophages, and tenocytes depending on the sample, while there were no statistically significant differences in proportions among samples (Figure 1G). Together, the abundance of high-quality cells in our dataset combined with rigorous data processing provides a useful compendium of transcriptionally annotated muscle mononuclear cell populations in rats conserved with age, reloading, and mechanical stimulation.

### Mechanotherapy Reprograms the FAP Transcriptome in Aged Rats During Recovery

We first focused our analysis on FAPs due to the observation of transcriptional heterogeneity identified in this study, and due to numerous reports implicating FAPs in the development of dysregulated ECM turnover, diabetes, fibrosis, and other muscle pathologies.[13,14,16,17] Using gene set enrichment analysis (GSA), we characterized FAP subclusters to numerous processes including *Collagen Biosynthesis*, *Matrix Metalloproteinase* (MMP) *Activation*, *Laminin Interactions*, and *Interleukin 6* (IL-6) *Signaling* (Figure 2A), which can broadly be summarized by both immuno- (*Csf1*; red) and ECM- (*Col1a1*; green) modulatory processes (Figure 2B). In order to determine whether age, reloading, or the use of mechanotherapy contributed to the transcriptional heterogeneity within FAPs, we subdivided the aggregate dataset and analyzed FAPs by each age and condition (Figure 2C). We found that the cluster of FAPs enriched with chemoattractant gene expression was specific to aged RE and aged REM FAPs only, as each of the other conditions annotated to clusters enriched in *Col1a1* expression (Figure 2A-C). To determine whether a subset of FAPs was responsible for the observed transcriptional heterogeneity, we performed sub-cluster analysis and reannotation of the aggregate FAP sample (Figure 2D). We found 3 populations of FAPs, similar to previous reports,[13,35] which could be segmented transcriptionally by unique expression of

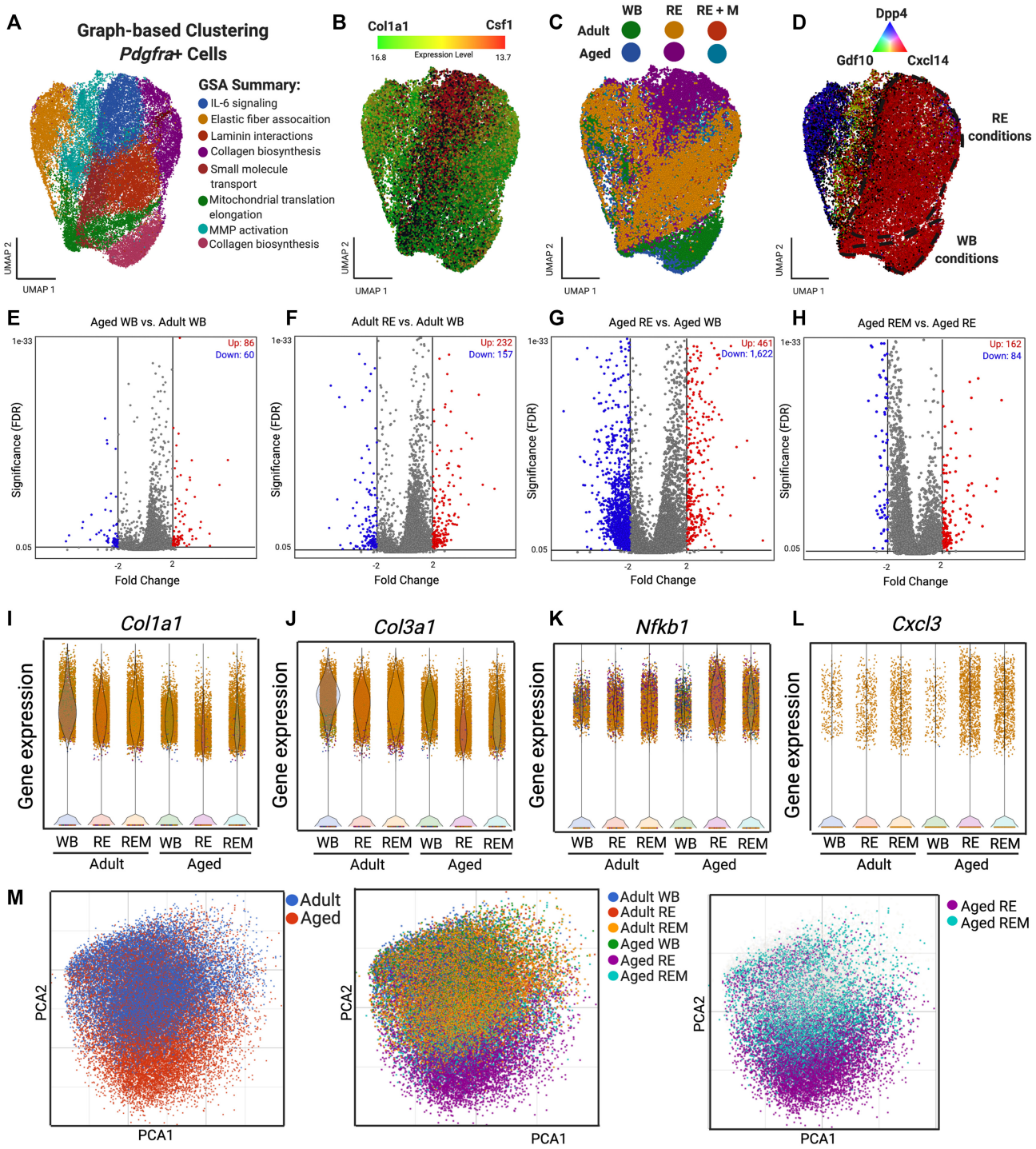


**Figure 2.** Mechanotherapy reprograms aged FAPs to gene expression similar to adult FAPs during recovery. (A) Unsupervised graph-based clustering of FAPs (37,175) for all samples. Reactome pathway analysis of each cluster using the top genes per cluster (FC>1.5; q-value<1.0E-5). (B) FAPs displayed by average gene expression of *Col1a1* (green) and *Csf1* (red), (C) by sample, and (D) by FAP subcluster populations. (E-H) Volcano plots of DEGs in FAPs (FC>2, -2; q-value<0.05). Upregulated in red, downregulated in blue and non-significant in gray. (I-L) Violin plots of *Col1a1*, *Col3a1*, *Nfkb1*, and *Cxcl3* gene expression. (M) PCA of FAPs colored by age (left panel), group (middle panel), and highlighted by aged RE and aged REM (right panel).

adipogenic lineage marker[35,44,45] dipeptidyl peptidase-4 (*Dpp4*; blue; Figure 2D), mesenchymal lineage marker[13] growth differentiation factor 10 (*Gdf10*; green; Figure 2D), and immunomodulatory marker[35] chemokine ligand 14 (*Cxcl14*; red; Figure 2D). Further analyses revealed that two *Cxcl14* subpopulations clustered separately based on ambulatory and recovery conditions, suggesting a specific role of *Cxcl14*+ FAPs in the recovery from atrophy (Figure 2C, 2D).

We further determined differentially expressed genes (DEGs) within FAPs in response to age, recovery and mechanotherapy,

by performing pseudo-bulk RNA-seq analysis of both the whole FAP population, along with the identified subclusters (Figure 2E-2H, Figure S1; FC +/− 2; q<0.05). Analysis of the bulk FAP population revealed a small number (86 up- and 60 downregulated) of DEGs between adult and aged muscle under ambulatory conditions. In adult muscle, there was a higher number of upregulated genes compared to down regulated with RE compared to WB (Figure 2F; 232 up- and 157 downregulated). By contrast, there was a substantial number of genes downregulated in aged RE muscle compared to aged WB conditions (Figure 2G; 461 up- and 1,622 downregulated genes). We found that mechanotherapy shifted the FAP transcriptome in the aged such that the number of upregulated DEGs was higher than the down regulated DEGs, compared to recovery alone (Figure 2H; 162 up- and 84 downregulated genes). Comparison of subclusters driving the observed differences in DEGs revealed that the *Cxcl14*+ fraction was solely responsible for the changes observed at the whole FAP population level (Figure S1), as there were no differences in the *Dpp4*+ nor *Gdf10*+ FAP fractions (data not shown), suggesting a specific role of immunomodulation in FAPs during the recovery from disuse atrophy.

We next performed targeted analyses of both ECM and inflammatory signaling genes relevant for ECM remodeling, to investigate the biological consequences of changes to the *Cxcl14*+ FAP transcriptome. There was a 2.5-fold reduction in *Col1a1* gene expression between aged and adult FAPs under ambulatory conditions, but there were no differences between adult WB and RE FAPs (Figure 2I). In contrast, FAP *Col1a1* gene expression was 3.2-fold lower in aged RE compared with aged WB, but was 2.3-fold higher in aged REM compared to aged RE alone (Figure 2I). For *Col3a1* gene expression, there were no differences between adult and aged WB, nor between adult WB and RE (Figure 2J). In contrast, *Col3a1* was 3.9-fold lower in aged RE compared to aged WB, but was 1.5-fold higher in aged REM compared to aged RE (Figure 2J). Notably, many of the top upregulated DEGs in FAPs between aged RE and aged WB were related to fibrosis, including connective tissue growth factor (*Ccn2*), tissue inhibitor of MMPs 1 (*Timp1*), and lysyl oxidase (*Lox*)[46–48] (Figure S2). *Timp1* was 4.3-fold and *Lox* was 2.3-fold higher in aged RE FAPs compared to WB, respectively (Figure S2). Mechanotherapy was associated with 1.6-fold lower gene expression of both *Timp1* and *Lox* expression in the aged, compared to RE alone (Figure S2). *Ccn2* expression was 3.6-fold higher in FAPs in aged compared to adult under WB conditions, which remained higher under both RE and REM conditions in the aged (Figure S2). Inflammatory genes were higher in aged RE compared to aged WB, including a 6.8- and 2.4-fold higher expression of nuclear factor kappa B subunit 1 (*Nfkb1*) and chemokine ligand 3 (*Cxcl3*), respectively (Figure 2K, 2L); mechanotherapy was associated with 1.8-fold lower gene expression of both *Nfkb1* and *Cxcl3* in aged FAPs recovering from disuse compared to RE (Figure 2K, 2L).

Last, we performed PCA of the aggregate FAP cluster, in order to determine whether mechanotherapy stimulates the FAP transcriptome in aged REM muscle similar to that of younger muscle. There was a clear distinction between the FAP clustering of aged and adult FAPs, highlighting the influence of age on the transcriptional landscape of FAPs (Figure 2M; left panel). However, the aged RE group was solely responsible for the variance in gene expression between adult and aged FAPs (Figure 2M; middle panel). Indeed, we found that mechanotherapy promoted a shift in the FAPs transcriptome more similar to that of adult RE muscle (Figure 2M; right panel). Collectively, these data demonstrate that in adult muscle during recovery from atrophy, FAPs appropriate gene expression towards ECM remodeling. In contrast, FAPs in muscle from aged rats recovering from atrophy exhibit gene expression related to immunomodulation, which is redirected towards ECM regulation following mechanotherapy.

## Skeletal Muscle Intercellular Communication with Aging, Recovery, and Mechanotherapy

We used receptor-ligand (RL) network analysis across experimental conditions to infer intercellular communication based on previous work demonstrating an impaired immune response in aged muscle recovering from disuse,[49,50] and our study identifying chemotaxis in aged RE FAPs. We identified the predominant transcriptional signaling axes between cells through integration of known RL interactions[34,35] with expression matrices of annotated mononuclear cell populations, and filtration for highly significant interactions (FC +/-3; q<0.01). We found that the predominant signaling axis in adult WB muscle was between FAPs, pericytes, and ECs (Figure 3A; Data File S1; # of RL pairs indicated redundantly by edge thickness and heatmap). Notably, the most abundant RL pair in adult muscle under WB conditions was between FAP expression of Wnt-5a (*Wnt5a*) and pericyte expression of melanoma cell adhesion molecule (*Mcam*), suggesting that FAPs may be involved in coordinating the migration of pericytes[51] (Figure 3A; Data File S1). In adult muscle recovering from disuse, the signaling milieu expanded from FAPs, pericytes and ECs to include satellite cells (SCs), macrophages, natural killer cells (NKs) and antigen presenting cells (APCs) (Figure 3B, Data File S2). Indeed, the top RL pair between top interactors in adult RE muscle was between vitronectin (*Vtn*) expression from pericytes and tumor necrosis factor receptor 1 (*Tnfrsf1*) expression from FAPs, potentially suggesting pericyte mediated expansion of the *Cxcl14*+ FAP fraction (Figure 3B; Data File S2). Following mechanotherapy in adult muscle, the top interaction was also between FAPs and pericytes, characterized by FAP expression of *Col3a1* and pericyte expression of integrin alpha A1 (*Itga1*), highlighting the mechanical influence of mechanotherapy on cellular mechanosensors (Figure 3C, Data File S3).

In the aged, the predominant signaling interactions under WB conditions included ECs, pericytes, macrophages, APCs, and T cells, with macrophages to APCs represented as the top interactors (Figure 3D, Data File S4). In aged WB muscle, granulocyte expression of secretory leukocyte protease inhibitor (*Slpi*) and macrophage expression of *Cd4* was the top RL pair (Figure 3D, Data File S4), suggesting stimulation of the innate immune response, which is frequently reported in aged tissues.[52] In aged RE muscle, the top interactors were macrophages to T cells, macrophages to NKs, and macrophages to APCs, demonstrating a pronounced inflammatory environment in aged muscle recovering from disuse (Figure 3E, Data File S5). The top RL pair in aged RE muscle was macrophage expression of interleukin 27b heterodimer Epstein-barr virus induced gene 3 (*Eib3*) and T cell expression of the IL-27 receptor alpha (*Il27ra*) (Figure 3E, Data File S5), suggesting a role for macrophage mediated skewing of the T cell compartment in the aging recovery from disuse.[53] Importantly following mechanotherapy in aged muscle, the signaling milieu of aged REM resembled that of adult RE and adult REM, as the top interactors were ECs to pericytes (Figure 3F, Data File S6). Indeed, the top interaction of aged REM ECs and pericytes was EC-derived delta-like canonical notch ligand 4 (*Dll4*) and pericyte expression of notch receptor 3 (*Notch3*), potentially suggesting mechanotherapy-promoted vascularization in aged muscle recovering from disuse (Figure 3F; Data File S6). A full atlas of RL

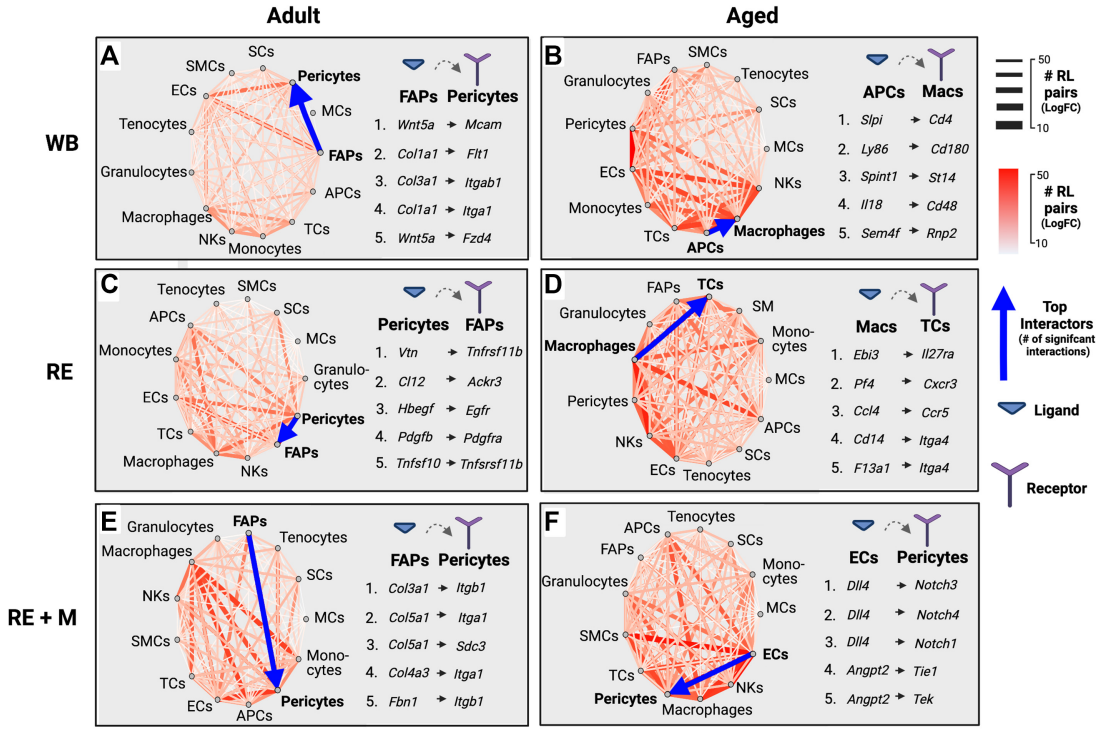


**Figure 3.** Receptor-ligand interaction analysis reveals age-related differences to chemotactic signaling during the recovery from disuse. Receptor-ligand network analysis of adult (A-C) and aged (D-F) muscle between weight-bearing (WB), recovery following disuse (RE), and recovery with mechanotherapy (REM) conditions (cutoff for significant interactions: q-value<0.001). The number of significant interactions is indicated both by color intensity and edge thickness. The top five RL interactions for each age and condition indicated to the right of interaction plot. Blue arrow indicates top cellular interactors with directionality indicating ligand→receptor.

interactions for mononuclear cell populations, age, and condition is provided in Supplemental Data Files S1-S6. Together, RL analyses allow us to infer a homeostatic FAP-pericyte-EC axis which remains intact in adult muscle regardless of recovery or mechanotherapy conditions. In aged tissue, however, the homeostatic axis of FAP-pericyte-EC is perturbed by immune cell signaling,[49,50] and is reestablished by mechanotherapy application.

## Mechanotherapy Reconditions Macrophage Dynamics in Aged Muscle During Recovery

We next focused our analyses on macrophages, as RL signaling in aged muscle in this study indicated an immune cell involvement and because an impaired immune cell response to aged muscle following from disuse has been recently reported.[49,50] Dimensionality reduction and visualization of macrophages revealed transcriptional segregation of cells based on expression of "M2" macrophage marker, *Cd163*, and phagocytic-related genes (data not shown). However, the use of the "M1/M2" designation is regarded as an oversimplication of macrophage plasticity, and macrophages are instead described by the preferred metabolic pathway.[54] Therefore, we utilized the KEGG database (https://www.genome.jp/kegg/brite.html) and used pathways of interest to calculate pathway activity scores,[36] which included the *Pentose Phosphate Pathway* and *Oxidative Phosphorylation*, corresponding to inflammatory[54] and anti-inflammatory macrophages,[55] respectively (Figure 4A). We also included gene sets annotated to *IL-17 Signaling*, *Phagosome*, and *ECM Regulators*, to infer both inflammatory status and cellular function between ages and conditions (Figure 4A). In adult RE macrophages, we found few differences in pathway activity scores compared to adult WB macrophages (Figure 4A). Mechanotherapy in adult macrophages resulted in higher pathway activity in both *Pentose Phosphate* and *Oxidative Phosphorylation*, along with higher scores for *ECM Regulators* gene sets (Figure 4A). In aged RE macrophages, we found a robust rise in *IL-17 Signaling* pathway activity with concomitant rises in *Phagosome* pathway activity, suggestive of a pro-inflammatory microenvironment (Figure 4A). Following mechanotherapy, we found that *IL-17 Signaling* was lower in aged REM macrophages, with a corresponding rise in pathway activity related to *Pentose Phosphate*, *Oxidative Phosphorylation*, and *ECM Regulators* (Figure 4A). Together, these data suggest an inflammatory macrophage response in aged RE muscle that is reconditioned towards a restorative transcriptional phenotype by mechanotherapy.

Last, we performed trajectory inference analysis[37] to determine whether mechanotherapy aligns aged macrophages with a trajectory similar to that of adult RE macrophages (Figure 4B-4D). Construction of lineage trajectories and initiation of pseudotime from ambulatory conditions identified a total of three trajectories (Figure 4B). Of the three trajectories identified, one of the identified trajectories was formed solely by aged RE macrophages, while the other two trajectories were equally comprised of the remaining macrophage populations (Figure 4B). Targeted analyses of the "drivers" for lineage and pseudotime progression revealed the three trajectories were formed based on unique expression of ECM remodeling (Fibronectin (*Fn1*); green), inflammation (Nuclear Factor Kappa B Subunit 1 (*Nfkb1*); red), and proliferative conditions (Jun Proto-Oncogene (*Jun*); blue) (Figure 4C). In aged RE macrophages, a single trajectory defined by inflammatory conditions was identified, which was reprogrammed by mechanotherapy towards trajectories defined by ECM remodeling and proliferation (Figure 4C and D). Collectively, these data demonstrate the ability of mechanotherapy to reduce gene expression related to pro-inflammatory

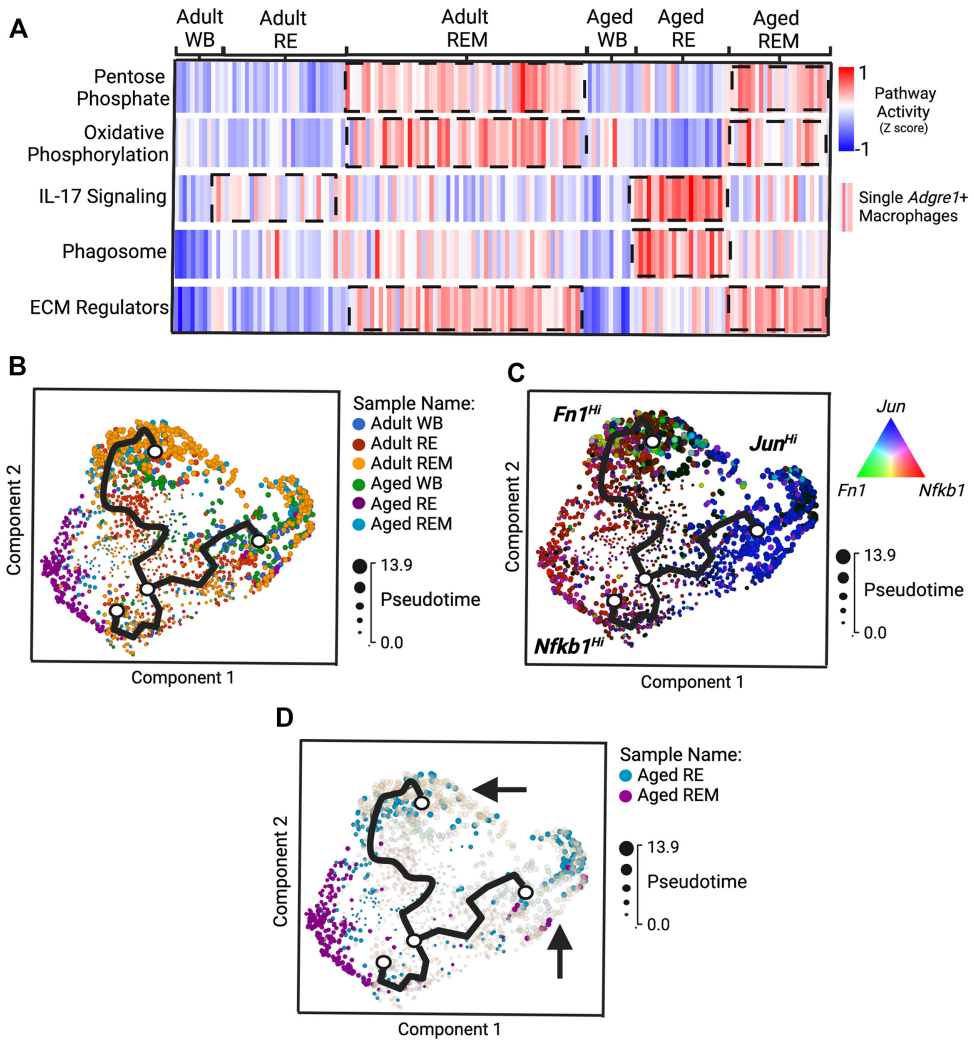


**Figure 4.** Mechanotherapy reprograms macrophage dynamics in the aged similar to that of adult macrophages recovering from disuse. (A) Pathway "activity scores" between ages and conditions calculated using AuCell[36] and visualized by heatmap (high "activity" shown in red, low "activity" shown in blue). Trajectory inference analysis using Monocle 3.0 displayed by sample (B), by "drivers" of pseudotime trajectories (C), and highlighted by aged RE and REM samples (D).

signaling of macrophages during recovery from disuse in aged, and instead enrich for genes involved in ECM remodeling in macrophage transcriptomes.

## Mechanotherapy Promotes ECM Remodeling in Aged Muscle During Recovery

In order to verify whether the observed transcriptional changes induced by recovery and mechanotherapy reflect phenotypic ECM remodeling, we measured mature collagen abundance (PSR), glycoprotein abundance (WGA), degraded collagen abundance (CHP) and *in vivo* collagen fractional synthetic rate (FSR) using stable isotope tracing in a separate cohort on rats (n = 6-8). To identify mature collagen, muscle sections were stained with picrosirius red (PSR) (Figure 5A) and analyzed under bright field and polarized light (Figure 5B); green corresponds to collagen in parallel with muscle fibers, red represents collagen networks perpendicular to muscle fibers and yellow is intermediate between green and red (Figure 5B).[8,56] The ratio of color densities was not different between groups in adult (Figure 5E) or aged rats (Figure 5F). However, we found that the amount of total birefringent (mature) collagen was higher in aged RE animals compared with aged WB and was lower in aged REM compared to aged RE, indicative of remodeling (Figure 5F). Muscle sections were stained with wheat germ agglutinin (WGA) to determine changes in ECM glycoprotein abundance (Figure 5C, G, H).[57] There were no differences in WGA abundance between any groups in adult animals (Figure 5G). However, aged rats receiving mechanotherapy during recovery had a lower abundance of WGA compared to both WB and RE conditions (Figure 5H). To determine the amount of degraded collagen, we measured the abundance of collagen hybridizing peptide (CHP; green, Figure 5D, I, J), which binds to unwound collagen fragments.[58] In adult rats, there was lower CHP abundance following mechanotherapy compared to ambulatory conditions (Figure 5I), while there were no differences between adult RE and adult REM rats (Figure 5I). In aged rats, there was lower abundance of CHP in the mechanotherapy group compared to both RE and WB conditions (Figure 5J), further indicative of remodeling. Lastly, there were no differences in collagen FSR in adult animals between any of the groups (Figure 5K) and in aged there was a trend ($p = 0.08$) for REM to be higher than WB (Figure 5L). Taken together, no change in collagen synthesis, lower levels of degraded collagen, and remodeling of ECM collagen/glycoprotein content suggest

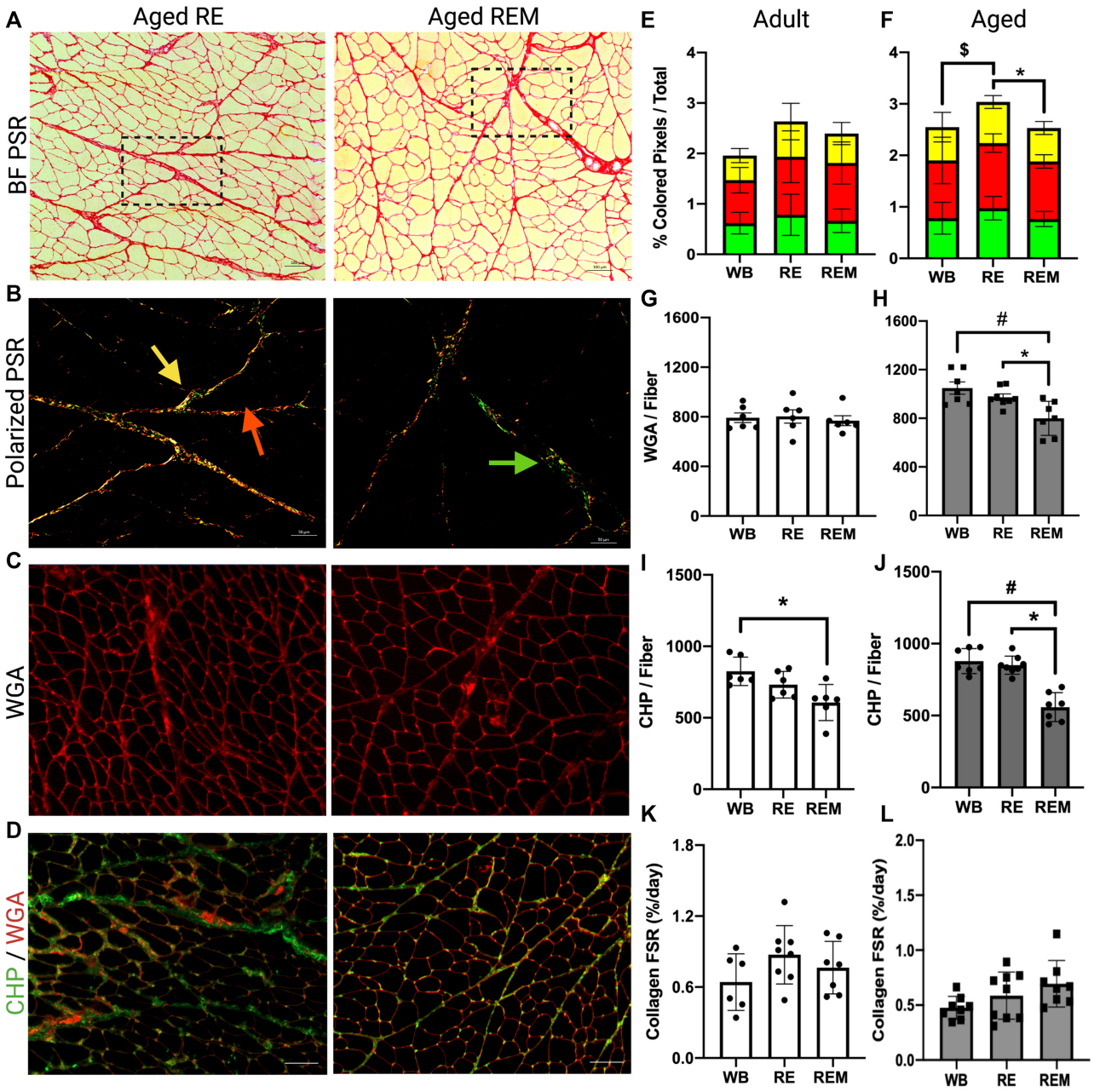


**Figure 5.** The effect of mechanotherapy on ECM remodeling in aged muscle during the recovery from disuse. Representative images of aged RE and aged REM picrosirius red under (A) bright-field (inlet indicated) and (B) polarized light, (C) WGA, and (D) CHP. Birefringent collagen is indicated by red, green, and yellow arrows (B). Quantification of PSR-Pol analysis between adult (E) and aged (F) WB, RE, and REM samples. Quantification of WGA analysis between adult (G) and aged (H) WB, RE, and REM samples. Quantification of CHP abundance relative to muscle fiber number between adult (I) and aged (J) WB, RE, and REM samples. Quantification of collagen FSR/day between (K) adult and (L) aged WB, RE, and REM samples. Scale bar is 100 $\mu$m. N = 6-8. $ refers to different from WB compared to RE. * refers to different from RE compared to REM. # refers to different from WB compared to REM. P<0.05. Values are means ± SEM.

mechanotherapy-mediated turnover of the ECM in aged muscle recovering from atrophy, and demonstrate physiological relevance of transcriptional findings.

## DISCUSSION

Results presented herein indicate that there is altered transcriptional regulation in aged muscle recovering from disuse atrophy, due to immunomodulation of ECM-regulating stromal cell populations. In addition, mechanotherapy reprograms these cells by lowering inflammation-related gene expression and elevating ECM-related gene expression, thereby enhancing ECM remodeling in aged muscle during recovery. Resolution of inflammation and remodeling of the ECM are important for gains in muscle size;[5,12,50] our results show transcriptional impairments to both of these processes in aged muscle during recovery, which are restored by mechanotherapy. Importantly, as we have previously shown that mechanotherapy (4.5 N) has no effect on muscle protein synthesis in the same experimental paradigm (4 bouts of mechanotherapy, 7 days of recovery,[30]), these results suggest remodeling of the ECM may be a prerequisite to changes in muscle size during recovery in the aged. We conclude that

the immunomodulatory effect of mechanotherapy is beneficial for aged skeletal muscle recovering from disuse by mechanically stimulating cell populations to restore ECM remodeling to levels similar to that of adult muscle.

## The Influence of Age on Cellular Dynamics During the Recovery from Disuse Atrophy

Our results highlight the complex interplay of non-myogenic cell populations during the recovery from disuse atrophy, which is influenced by age. Moreover, we show that the recovery from disuse atrophy is a far more complex process than simply increasing myofiber mass, but rather a highly orchestrated initiation and resolution of inflammation and ECM remodeling, both of which create a microenvironment permissive to gains in muscle size.[12,49,50] In our study, we identified macrophage transcriptomes enriched with pro-inflammatory factors, with notably reduced expression related to ECM regulation in aged RE muscle compared to adult RE. Indeed, Reidy and colleagues have shown an impaired macrophage response in aged muscle recovering from disuse, with a reduction of absolute macrophage abundance, that corresponded with delayed and/or incomplete recovery.[50] It was concluded that aged muscle macrophages are either intrinsically impaired relative to adult muscle macrophages, or there is a difference in chemotactic recruitment from muscle-resident cell populations in aged muscle.[50] Our study provides a novel explanation extrinsic to impaired macrophage dynamics in aged muscle, as aged FAPs display an impairment and/or delay in enhancing chemotactic signaling to infiltrating immune cells relative to younger skeletal muscle. While there is evidence of expansion of the FAP population pool during the recovery from muscle injury,[16,35,59] this is the first study to implicate FAPs in the recovery from disuse, particularly at the presented timepoint. Temporal experiments will be useful in the future to determine if aged muscle FAPs are responsible for reduced ECM regulation regardless of the stage of recovery, or rather the cellular kinetics of recovery (i.e. FAP immunomodulation and/or ECM remodeling) are delayed in aged relative to adult muscle.

A critical barrier to identifying a mechanistic understanding of the age-related impairment to the recovery from disuse atrophy is the inability to recapitulate the aged microenvironment, which is reflected by a complex combination of signaling axes between skeletal muscle fibers, the stromal cellular environment, and infiltrating cell populations. Moreover, the sequalae of signaling cascades that occur in each cell population likely occur temporally in a step-wise fashion, i.e. as a result of intercellular communication, which cannot be captured by current methods. RL network analysis was used in our study to bypass these obstacles and infer a pro-inflammatory landscape of mononuclear cells based on enrichment of known RL pairs. A homeostatic RL signaling axis was identified between FAPs, pericytes, and ECs, which predominates across conditions in adult muscle. During RE in adult muscle, pro-inflammatory signaling axes from the stroma associates with elevated immune cell gene expression related to phagocytosis. In aged muscle under both ambulatory and recovery conditions, enhanced inflammatory signaling of numerous stromal and infiltrating cell populations associated with poor muscle mass recovery.[30] Following the application of mechanotherapy, signaling axes in aged muscle resembled that of younger muscle: there was enhanced interaction between the endothelium and perivascular cells, which has been reported to result in improved functional outcomes during the recovery from disuse.[60] Taken together, our results not only implicate altered crosstalk between skeletal muscle stromal cell populations with circulating immune cells in aged muscle during recovery, they also demonstrate that the transcriptomes of stromal/circulating cells can be influenced by mechanotherapy.

## Mechanotherapy as an Immunomodulator During the Recovery from Disuse in Aged Muscle

The use of massage-like therapies to enhance muscle recovery following an insult through immunomodulation has been reported previously.[21,23] Following a bout of damaging eccentric contractions, Butterfield et al. showed that massage-like cyclic compressive loading attenuated immune cell infiltration and accelerated the recovery of peak isometric torque in rabbits.[23] In humans, Crane et al. showed that massage therapy applied after a damaging bout of exercise attenuated the rise of pro-inflammatory cytokines and promoted mitochondrial biogenesis.[21] In our study, we demonstrated that mechanotherapy has the potential to beneficially affect numerous components of the ECM in aged muscle during recovery, while also providing a cellular systems-level insight into processes underlying our phenotypic findings. Indeed, we found that mechanotherapy is immunomodulatory to aged skeletal muscle recovering from disuse, in part by repurposing the FAP transcriptome from chemotaxis-related gene expression to ECM remodeling, and by introducing a macrophage transcriptome associated with phagocytic activity. A similar mechanism has been proposed by Fix and colleagues, who demonstrated that administration of an immunomodulatory secretory product derived from pluripotent stem cells to aging mouse muscle recovering from disuse, curbed inflammation, promoted ECM turnover, and enhanced muscle size.[61] Here, we show that ECM remodeling is enhanced following mechanotherapy treatment during aged recovery, as evidenced by reduced proteoglycan and collagen abundance. There are three lines of evidence suggesting mechanotherapy promotes breakdown of the ECM during remodeling. First, collagen synthesis was unchanged in this study, despite elevated Col1a1 and Col3a1 gene expression in FAPs from aged REM muscle. Second, mechanotherapy caused reduced WGA, PSR, and CHP in this study, each are markers commonly used to study fibrosis.[8,57,58] Last, trajectory inference analysis of macrophages from aged REM muscle indicated that mechanotherapy elevates phagocytosis-related gene expression within myeloid cells, suggesting elevated uptake of ECM components during recovery. It is possible that the enhancement to ECM turnover and influence to macrophage dynamics by mechanotherapy in aged muscle will enhance muscle size, but at later timepoints than measured in this study. Evidence for this hypothesis is reflected in our previous work demonstrating no changes to muscle fiber size at the same timepoint in aged muscle.[30] As ECM turnover and resolution of inflammation are elements of the recovery process which precede gains in myofiber size,[12,61] it is possible that the enhancement to ECM remodeling in aged muscle by mechanotherapy, as shown herein, will result in enhanced muscle size as recovery proceeds. Future studies should be directed towards investigating whether the effect of mechanotherapy to promote muscle size recovery is delayed, rather than absent, relative to that of adult muscle.

The clinical potential of these findings is demonstrated by the significant burden disuse atrophy places on older adults, ultimately contributing to delayed rates of hospital discharge

and poor health outcomes.[62–64] Indeed, mechanotherapy may present as a promising addition to current rehabilitative strategies, ultimately accelerating functionally recovery, which associates with decreased mortality.[64] The fact that the intervention was so beneficial considering the low frequency and duration and relatively low force application makes it even more therapeutically attractive. Since mechanotherapy serves an immunomodulatory role during muscle recovery,[21,25,27] it is possible that massage-like interventions could be beneficial in several different clinical scenarios. Mechanotherapy may have the potential to enhance recovery processes such as more severe, regeneration-inducing injuries, in patients undergoing muscle wasting due to critical illness unable to ambulate, or those with cachexia unable to perform more traditional rehabilitative therapies. It is well documented that massage-like therapies are well tolerated in clinical settings,[65,66] and as the data from this study highlight, has potential to promote aspects of recovery, such as ECM remodeling. Currently ongoing clinical trials to investigate the efficacy of mechanotherapy on muscle wasting highlight the translation potential of these findings (ClinicalTrials.gov Identifier: NCT04131712). Taken together, mechanotherapy in the form of cyclic compressive loading reprograms ECM regulating cells in muscle to create a more growth-promoting environment through its immunomodulatory effect during the recovery from disuse in aged rats. Future studies should be directed towards investigating how the observed effects of mechanotherapy on immune and ECM remodeling processes can be used clinically to enhance recovery after skeletal muscle insults.

### Limitations and Future Directions

There are a few limitations to the current study. First, scRNA-seq and evaluation of the ECM was measured at a single timepoint, which prevents us from confidently determining whether aged animals have impaired or delayed recovery compared to adult muscle. However, the depth of analysis in the current study highlights previously unexplored aspects of the recovery from disuse, and opens up new possibilities for effective intervention of aging muscle. Second, it is unclear whether the transcriptional changes observed in muscles receiving mechanotherapy are due to a single bout or a repeated bout effect. However, the experimental design was selected in order to compare our current findings to our previous reports,[25,30,31] which strengthens our conclusions due to the ability to compare to previous findings. Third, much of the interpretation of intercellular signaling is based on transcriptomics of receptors and ligands and does not capture cell-cell communication utilizing other mechanisms, such as the release of small extracellular vesicles or direct cell-to-cell contact.[67,68] However, the insight gained from our receptor-ligand analysis not only provides a systems-level approach to infer intercellular communication, it also presents a resource to the muscle community on muscle mononuclear cell crosstalk. Finally, it is clear from the previous literature that age-related changes in the ECM are greatly affected by post-translational modifications (PTMs) such as covalent cross-linking of intramuscular collagen,[8,48,69,70] and transcriptomic analyses do not capture these processes. Despite this, our analyses assessing ECM turnover following mechanotherapy suggests our transcriptional findings bear physiological consequence in ECM remodeling.

In summary, we provide evidence for age-related dysregulation to the transcriptional landscape of muscle mononuclear cell populations critical to ECM remodeling, including FAPs and macrophages, ultimately contributing to an impaired immune response and remodeling of the ECM during the aged recovery from disuse. In addition, we show that mechanotherapy reprograms the transcriptomes of non-myogenic cell populations in aged muscle to similar transcriptional levels as adult muscle, thereby promoting regulation of the immune response and ECM remodeling similar to that of adult rats during the recovery from disuse atrophy.

## Supplementary Material

Supplementary material is available at the *APS Function* online.

## Acknowledgments

scRNA-seq analyses were performed using Partek Flow. All figures were prepared using Biorender. The authors would like to thank Stephanie Oprescu, MSc, and Shihuan Kuang, PhD at Purdue University for their assistance in RL network analyses. The authors would also like to thank Jamie Sturgill, PhD at the University of Kentucky for her assistance in immune cell characterization and interpretation.

## Author Contributions

Author contributions were determined using the CRediT model: Conceptualization: ZRH, BFM, TAB, EED. Methodology: ZRH, YAW, BDP, KM, ALC, MML, DAH, BFM, TAB, EED. Investigation: ZRH, YAW, KH, ALC, MML, BFM, TAB, EED. Visualization: ZRH, BFM, TAB, EED. Funding acquisition: BFM, TAB, EED. Project administration: BFM, TAB, EED. Supervision: BFM, TAB, EED. Writing – original draft: ZRH, DAH, BFM, TAB, EED. Writing – review & editing: ZRH, YAW, BDP, KM, ALC, DVP, MML, DAH, BFM, TAB, EED.

## Funding

National Center for Complementary and Integrative Health, National Institutes of Health grant RO1AT009268 (EED, TAB, BFM). National Institute on Aging, National Institutes of Health grant R21AG042699 (EED, TAB). National Center for Research Resources, National Center for Advancing Translational Science, National Institutes of Health grant UL1TR001998 (ZRH). National Center for Complementary and Integrative Health, National Institutes of Health grant F31AT01147201 (ZRH).

## Data Availability Statement

The data that support the findings of this study are available in the Gene Expression Omnibus under accession number GSE184413.

## References

1. English KL, Paddon-Jones D. Protecting muscle mass and function in older adults during bed rest. *Curr Opin Clin Nutr Metab Care*. 2010;**13**(1):34–39.
2. Hvid LG, Suetta C, Nielsen JH, et al. Aging impairs the recovery in mechanical muscle function following 4 days of disuse. *Exp Gerontol*. 2014;**52**:1–8.
3. Suetta C, Hvid LG, Justesen L, et al. Effects of aging on human skeletal muscle after immobilization and retraining. *J Appl Physiol*. 2009;**107**(4):1172–1180.

4. Reidy PT, Lindsay CC, McKenzie AI, et al. Aging-related effects of bed rest followed by eccentric exercise rehabilitation on skeletal muscle macrophages and insulin sensitivity. *Exp Gerontol*. 2018;**107**:37–49.
5. St Pierre BA, Tidball JG. Differential response of macrophage subpopulations to soleus muscle reloading after rat hindlimb suspension. *J Appl Physiol*. 1994;**77**(1):290–297.
6. Arnold L, Henry A, Poron F, et al. Inflammatory monocytes recruited after skeletal muscle injury switch into antiinflammatory macrophages to support myogenesis. *J Exp Med*. 2007;**204**(5):1057–1069.
7. Jarvinen TA, Jozsa L, Kannus P, Jarvinen TL, Jarvinen M. Organization and distribution of intramuscular connective tissue in normal and immobilized skeletal muscles. An immunohistochemical, polarization and scanning electron microscopic study. *J Muscle Res Cell Motil*. 2002;**23**(3):245–254.
8. Wood LK, Kayupov E, Gumucio JP, Mendias CL, Claflin DR, Brooks SV. Intrinsic stiffness of extracellular matrix increases with age in skeletal muscles of mice. *J Appl Physiol*. 2014;**117**(4):363–369.
9. Barberi L, Scicchitano BM, De Rossi M, et al. Age-dependent alteration in muscle regeneration: the critical role of tissue niche. *Biogerontology*. 2013;**14**(3):273–292.
10. Silver JS, Günay KA, Cutler AA, et al. Injury-mediated stiffening persistently activates muscle stem cells through YAP and TAZ mechanotransduction. *Sci Adv*. 2021;**7**(11):eabe4501.
11. Bajpai A, Li R, Chen W. The cellular mechanobiology of aging: from biology to mechanics. *Ann N Y Acad Sci*. 2020; doi: 10.1111/nyas.14529.
12. Garg K, Mahmassani ZS, Dvoretskiy S, et al. Laminin-111 Improves the Anabolic Response to Mechanical Load in Aged Skeletal Muscle. *J Gerontol A Biol Sci Med Sci*. 2021;**76**(4):586–590.
13. Uezumi A, Ikemoto-Uezumi M, Zhou H, et al. Mesenchymal Bmp3b expression maintains skeletal muscle integrity and decreases in age-related sarcopenia. *J Clin Invest*. 2021;**131**(1) doi: 10.1172/jci139617.
14. Schüler SC, Kirkpatrick JM, Schmidt M, et al. Extensive remodeling of the extracellular matrix during aging contributes to age-dependent impairments of muscle stem cell functionality. *Cell Rep*. 2021;**35**(10):109223.
15. Qiu X, Liu S, Zhang H, et al. Mesenchymal stem cells and extracellular matrix scaffold promote muscle regeneration by synergistically regulating macrophage polarization toward the M2 phenotype. *Stem Cell Res Ther*. 2018;**9**(1):88.
16. Stepien DM, Hwang C, Marini S, et al. Tuning Macrophage Phenotype to Mitigate Skeletal Muscle Fibrosis. *J Immunol*. 2020;**204**(8):2203–2215.
17. Farup J, Just J, de Paoli F, et al. Human skeletal muscle CD90(+) fibro-adipogenic progenitors are associated with muscle degeneration in type 2 diabetic patients. *Cell Metab*.2021;**33**(11):2201–2214.e10.e11.
18. Curran J. The Yellow Emperor's Classic of Internal Medicine. *Bmj*. © BMJ Publishing Group Ltd 2008.; 2008:777. vol. 7647.
19. Hentschel HD, Schneider J.[The history of massage in the ways of life and healing in India]. *Wurzbg Medizinhist Mitt*. 2004;**23**:179–203. Zur geschichte der massage in der indischen lebens- und heilweise.
20. Blunt E. Foot reflexology. *Holist Nurs Pract*. 2006;**20**(5):257–259.
21. Crane JD, Ogborn DI, Cupido C, et al. Massage therapy attenuates inflammatory signaling after exercise-induced muscle damage. *Sci Transl Med*. 2012;**4**(119):119ra13.
22. Waters-Banker C, Butterfield TA, Dupont-Versteegden EE. Immunomodulatory effects of massage on nonperturbed skeletal muscle in rats. *J Appl Physiol*. 2014;**116**(2):164–175.
23. Butterfield TA, Zhao Y, Agarwal S, Haq F, Best TM. Cyclic compressive loading facilitates recovery after eccentric exercise. *Med Sci Sports Exercise*. 2008;**40**(7):1289–1296.
24. Van Pelt DW, Lawrence MM, Miller BF, Butterfield TA, Dupont-Versteegden EE. Massage as a Mechanotherapy for Skeletal Muscle. *Exerc Sport Sci Rev*. 2021;**49**(2):107–114.
25. Miller BF, Hamilton KL, Majeed ZR, et al. Enhanced skeletal muscle regrowth and remodelling in massaged and contralateral non-massaged hindlimb. *J Physiol*. 2018;**596**(1):83–103.
26. Hunt ER, Confides AL, Abshire SM, Dupont-Versteegden EE, Butterfield TA. Massage increases satellite cell number independent of the age-associated alterations in sarcolemma permeability. *Physiol Rep*. 2019;**7**(17):e14200.
27. Lawrence MM, Van Pelt DW, Confides AL, et al. Massage as a mechanotherapy promotes skeletal muscle protein and ribosomal turnover but does not mitigate muscle atrophy during disuse in adult rats. *Acta physiologica*. 2020;**229**(3):e13460.
28. Van Pelt DW, Confides AL, Abshire SM, Hunt ER, Dupont-Versteegden EE, Butterfield TA. Age-related responses to a bout of mechanotherapy in skeletal muscle of rats. *J Appl Physiol*. 2019;**127**(6):1782–1791.
29. White JR, Confides AL, Moore-Reed S, Hoch JM, Dupont-Versteegden EE. Regrowth after skeletal muscle atrophy is impaired in aged rats, despite similar responses in signaling pathways. *Exp Gerontol*. 2015;**64**:17–32.
30. Lawrence MM, Van Pelt DW, Confides AL, et al. Muscle from aged rats is resistant to mechanotherapy during atrophy and reloading. *Geroscience*. 2020; doi:10.1007/s11357-020-00215-y.
31. Hettinger ZR, Hamagata K, Confides AL, et al. Age-Related Susceptibility to Muscle Damage Following Mechanotherapy in Rats Recovering From Disuse Atrophy. *The Journals of Gerontology: Series A*. 2021;**76**(12):2132–2140 doi:10.1093/gerona/glab186.
32. Miller BF, Wolff CA, Peelor FF, 3rd, Shipman PD, Hamilton KL. Modeling the contribution of individual proteins to mixed skeletal muscle protein synthetic rates over increasing periods of label incorporation. *J Appl Physiol*. 2015;**118**(6):655–661.
33. Liu L, Cheung TH, Charville GW, Rando TA. Isolation of skeletal muscle stem cells by fluorescence-activated cell sorting. *Nat Protoc*. 2015;**10**(10):1612–1624.
34. Ramilowski JA, Goldberg T, Harshbarger J, et al. A draft network of ligand-receptor-mediated multicellular signalling in human. *Nat Commun*. 2015;**6**:1, 7866.
35. Oprescu SN, Yue F, Qiu J, Brito LF, Kuang S. Temporal Dynamics and Heterogeneity of Cell Populations during Skeletal Muscle Regeneration. *iScience*. 2020;**23**(4): 100993.
36. Aibar S, González-Blas CB, Moerman T, et al. SCENIC: single-cell regulatory network inference and clustering. *Nat Methods*. 2017;**14**(11):1083–1086.
37. Trapnell C, Cacchiarelli D, Grimsby J, et al. The dynamics and regulators of cell fate decisions are revealed by pseudotemporal ordering of single cells. *Nat Biotechnol*. 2014;**32**(4):381–386.
38. Qiu X, Hill A, Packer J, Lin D, Ma YA, Trapnell C. Single-cell mRNA quantification and differential analysis with Census. *Nat Methods*. 2017;**14**(3):309–315.
39. Miller BF, Olesen JL, Hansen M, et al. Coordinated collagen and muscle protein synthesis in human patella tendon and

quadriceps muscle after exercise. *J Physiol*. 2005;**567**(3):1021–1033.
40. Petrosino JM, Leask A, Accornero F. Genetic manipulation of CCN2/CTGF unveils cell-specific ECM-remodeling effects in injured skeletal muscle. *FASEB J*. 2019;**33**(2): 2047–2057.
41. Arruda EM, Mundy K, Calve S, Baar K. Denervation does not change the ratio of collagen I and collagen III mRNA in the extracellular matrix of muscle. *Am J Physiol Regul Integr Comp Physiol*. 2007;**292**(2):R983–R987.
42. Rubenstein AB, Smith GR, Raue U, et al. Single-cell transcriptional profiles in human skeletal muscle. *Sci Rep*. 2020;**10**(1):229.
43. Xu Z, You W, Chen W, et al. Single-cell RNA sequencing and lipidomics reveal cell and lipid dynamics of fat infiltration in skeletal muscle. *J Cachexia Sarcopenia Muscle*. 2021;**12**(1):109–129.
44. De Micheli AJ, Laurilliard EJ, Heinke CL, et al. Single-Cell Analysis of the Muscle Stem Cell Hierarchy Identifies Heterotypic Communication Signals Involved in Skeletal Muscle Regeneration. *Cell Rep*. 2020;**30**(10):3583–3595.e5.
45. Scott RW, Arostegui M, Schweitzer R, Rossi FMV, Underhill TM. Hic1 Defines Quiescent Mesenchymal Progenitor Subpopulations with Distinct Functions and Fates in Skeletal Muscle Regeneration. *Cell Stem Cell*. 2019;**25**(6): 797–813.e9.
46. Sun G, Haginoya K, Chiba Y, et al. Elevated plasma levels of tissue inhibitors of metalloproteinase-1 and their overexpression in muscle in human and mouse muscular dystrophy. *J Neurol Sci*. 2010;**297**(1-2):19–28.
47. Dorn LE, Petrosino JM, Wright P, Accornero F. CTGF/CCN2 is an autocrine regulator of cardiac fibrosis. *J Mol Cell Cardiol*. 2018;**121**:205–211.
48. Haus JM, Carrithers JA, Trappe SW, Trappe TA. Collagen, cross-linking, and advanced glycation end products in aging human skeletal muscle. *J Appl Physiol*. 2007;**103**(6):2068–2076.
49. Fix DK, Ekiz HA, Petrocelli JJ, et al. Disrupted macrophage metabolic reprogramming in aged soleus muscle during early recovery following disuse atrophy. *Aging Cell*. 2021;**n/a**(n/a):e13448.
50. Reidy PT, McKenzie AI, Mahmassani ZS, et al. Aging impairs mouse skeletal muscle macrophage polarization and muscle-specific abundance during recovery from disuse. *Am J Physiol Endocrinol Metab*. 2019;**317**(1): E85–E98.
51. Witze ES, Litman ES, Argast GM, Moon RT, Ahn NG. Wnt5a control of cell polarity and directional movement by polarized redistribution of adhesion receptors. *Science*. 2008;**320**(5874):365–369.
52. Gomez CR, Nomellini V, Faunce DE, Kovacs EJ. Innate immunity and aging. *Exp Gerontol*. 2008;**43**(8):718–728.
53. Tidball JG, Flores I, Welc SS, Wehling-Henricks M, Ochi E. Aging of the immune system and impaired muscle regeneration: A failure of immunomodulation of adult myogenesis. *Exp Gerontol*. 2021;**145**:111200.
54. Tannahill GM, Curtis AM, Adamik J, et al. Succinate is an inflammatory signal that induces IL-1$\beta$ through HIF-1$\alpha$. *Nature*. 2013;**496**(7444):238–242.
55. Du L, Lin L, Li Q, et al. IGF-2 Preprograms Maturing Macrophages to Acquire Oxidative Phosphorylation-Dependent Anti-inflammatory Properties. *Cell Metab*. 2019;**29**(6):1363–1375.e8.e8.
56. Junqueira LC, Bignolas G, Brentani RR. Picrosirius staining plus polarization microscopy, a specific method for collagen detection in tissue sections. *Histochem J*. 1979;**11**(4): 447–455.
57. Emde B, Heinen A, Gödecke A, Bottermann K. Wheat germ agglutinin staining as a suitable method for detection and quantification of fibrosis in cardiac tissue after myocardial infarction. *Eur J Histochem*. 2014;**58**(4):2448.
58. Abramowitz MK, Paredes W, Zhang K, et al. Skeletal muscle fibrosis is associated with decreased muscle inflammation and weakness in patients with chronic kidney disease. *Am J Physiol Renal Physiol*. 2018;**315**(6):F1658–F1669.
59. Joe AW, Yi L, Natarajan A, et al. Muscle injury activates resident fibro/adipogenic progenitors that facilitate myogenesis. *Nat Cell Biol*. 2010;**12**(2):153–163.
60. Munroe M, Dvoretskiy S, Lopez A, et al. Pericyte transplantation improves skeletal muscle recovery following hindlimb immobilization. *FASEB J*. 2019;**33**(6):7694–7706.
61. Fix DK, Mahmassani ZS, Petrocelli JJ, et al. Reversal of deficits in aged skeletal muscle during disuse and recovery in response to treatment with a secrotome product derived from partially differentiated human pluripotent stem cells. *Geroscience*. 2021;**43**(6):2635–2652.
62. Hall MJ, DeFrances CJ, Williams SN, Golosinskiy A, Schwartzman A. National Hospital Discharge Survey: 2007 summary. *Natl Health Stat Report*. 2010;(29):1–20, 24.
63. Corcoran PJ. Use it or lose it–the hazards of bed rest and inactivity. *West J Med*. 1991;**154**(5):536–8.
64. Ostir GV, Berges IM, Kuo YF, Goodwin JS, Fisher SR, Guralnik JM. Mobility activity and its value as a prognostic indicator of survival in hospitalized older adults. *J Am Geriatr Soc*. 2013;**61**(4):551–557.
65. Vergo MT, Pinkson BM, Broglio K, Li Z, Tosteson TD. Immediate Symptom Relief After a First Session of Massage Therapy or Reiki in Hospitalized Patients: A 5-Year Clinical Experience from a Rural Academic Medical Center. *J Altern Complement Med*. 2018;**24**(8):801–808.
66. Chase T, Jha A, Brooks CA, Allshouse A. A pilot feasibility study of massage to reduce pain in people with spinal cord injury during acute rehabilitation. *Spinal Cord*. 2013;**51**(11):847–851.
67. Murach KA, Peck BD, Policastro RA, et al. Early satellite cell communication creates a permissive environment for long-term muscle growth. *iScience*. 2021;**24**(4):102372.
68. Fry CS, Kirby TJ, Kosmac K, McCarthy JJ, Peterson CA. Myogenic Progenitor Cells Control Extracellular Matrix Production by Fibroblasts during Skeletal Muscle Hypertrophy. *Cell Stem Cell*. 2017;**20**(1):56–69.
69. Reddy GK. Cross-linking in collagen by nonenzymatic glycation increases the matrix stiffness in rabbit achilles tendon. *Exp Diabesity Res*. 2004;**5**(2):143–153.
70. Abbott CB, Lawrence MM, Kobak KA, et al. A novel stable isotope approach demonstrates surprising degree of age-related decline in skeletal muscle collagen proteostasis. *Function*.**2**, 4, 2021; doi:10.1093/function/zqab028